



Heterogeneous & Homogeneous & Bio- & Nano-

CHEM**CAT**CHEM

CATALYSIS

Accepted Article

Title: Effect of crystallographic phase of ruthenium nanosponges on arene and substituted arene hydrogenation activity

Authors: Balaji Rao Jagirdar and Sourav Ghosh

This manuscript has been accepted after peer review and appears as an Accepted Article online prior to editing, proofing, and formal publication of the final Version of Record (VoR). This work is currently citable by using the Digital Object Identifier (DOI) given below. The VoR will be published online in Early View as soon as possible and may be different to this Accepted Article as a result of editing. Readers should obtain the VoR from the journal website shown below when it is published to ensure accuracy of information. The authors are responsible for the content of this Accepted Article.

To be cited as: *ChemCatChem* 10.1002/cctc.201800287

Link to VoR: <http://dx.doi.org/10.1002/cctc.201800287>

WILEY-VCH

www.chemcatchem.org



Effect of crystallographic phase of ruthenium nanosponges on arene and substituted arene hydrogenation activity

Sourav Ghosh and Balaji R. Jagirdar*

Abstract: Identifying crystal structure sensitivity of a catalyst for a particular reaction is an important issue in heterogeneous catalysis. In this context, the activity of different phases of ruthenium catalysts for benzene hydrogenation has not been investigated as yet. The synthesis of hcp and fcc phases of ruthenium nanosponges by chemical reduction method has been described. Reduction of ruthenium chloride using ammonia borane (AB) and tert-butylamine borane (TBAB) as reducing agents gave ruthenium nanosponge in its hcp phase. On the other hand, reduction using sodium borohydride (SB) afforded ruthenium nanosponge in its fcc phase. The as prepared hcp ruthenium nanosponge was found to be catalytically more active compared to the as prepared fcc ruthenium nanosponge for hydrogenation of benzene. The hcp ruthenium nanosponge was found to be thermally stable and recyclable over several cycles. This self-supported hcp ruthenium nanosponge shows excellent catalytic activity towards hydrogenation of various substituted benzenes. Moreover, the ruthenium nanosponge catalyst was found to bring about selective hydrogenation of aromatic cores of phenols and aryl ethers to the respective alicyclic products without hydrogenolysis of the C–O bond.

Introduction

In heterogeneous catalysis, the catalytic activity is governed by several parameters, such as active phase composition, particle size, crystal structure, morphology, and support.^[1] In case of self-supported metals, namely metal nanosponges, the effect of the support can be eliminated and therefore, for a particular morphology of the material the activity solely depends on the crystal structure of the metal.^[1] On the other hand, crystallographic phase of a material is an important parameter wherein, change in the crystal phase can lead to different physicochemical properties. Over decades, identifying the crystal structure sensitivity of catalysts in chemical reactions to accomplish maximum productivity remains one of the most significant yet challenging issues in heterogeneous catalysis.^[2] A notable example of such structure sensitivity is the Fischer-Tropsch synthesis (FTS) wherein, various in situ characterizations and theoretical calculations were conducted to understand the crystal structure sensitivity for cobalt, ruthenium, and iron catalysts.^[2-4] Apart from Fischer-Tropsch synthesis, several other chemical and electrochemical reactions wherein, the crystallographic phase of metal catalysts influence the catalytic processes have been investigated.^[5]

Hydrogenation of benzene was first accomplished over finely divided nickel particles by Sabatier and Senderens way back in the 19th century.^[6,7] The field of arene hydrogenation flourished ever since.^[8-10] Selective hydrogenation of substituted arenes to their respective alicyclic derivatives is one of the most important reactions carried out in the industry for generation of various intermediates that are important precursors for the production of polymers, dyes, and fine chemicals.^[11-16] Industrially, monocyclic arene hydrogenation is typically performed under harsh conditions (high pressure and high temperature) using heterogeneous transition metal catalysts, such as Rh/Al₂O₃ and Raney nickel.^[10,17] In case of metal based catalysts, ruthenium catalysts are preferred over other precious metal catalysts, such as rhodium, iridium, and platinum because of its moderate cost and high catalytic activity. Among the many homogeneous and heterogeneous ruthenium catalysts, homogeneous small molecule based catalysts whose true nature (homogeneous or heterogeneous colloidal particles) is still under scrutiny, show poor activity.^[9,18,19] On the other hand, surfactant and ionic liquid stabilized ruthenium nanoparticles and supported (MOFs, polymers, dendrimers, metal oxides) ruthenium nanoparticles were found to be catalytically active for arene hydrogenation reaction.^[9,20-37] Although, several heterogeneous ruthenium nanostructures were reported for hydrogenation of derivatives of benzene, yet the influence of the crystallographic phase of ruthenium on hydrogenation of arenes has not been explored.

In this context, self-supported porous metal offers a unique opportunity to eliminate the support effects and helps to determine the true origin of the catalytic activity of different phases of pure metal. Porous metals are of immense interest in the field of heterogeneous catalysis because of its high surface area and the pores which facilitate easy diffusion of the substrates within the accessible surface active sites of the materials.^[38,39] Fabrication of three dimensional bicontinuous porous metals in which pores are interconnected is quite challenging.^[40] Porous metals synthesized by conventional approaches such as template synthesis and dealloying method suffer from scalability issues and these are multistep synthetic procedures as well as, are metal specific.^[40-45] Recently, these problems were overcome by carrying out the assembly of ex-situ or in-situ prepared nanoparticles.^[46-51] Eswaramoorthy's group and others reported an in-situ assembly of nanoparticles for the synthesis of high surface area metal nanosponges.^[49-51] Herein, we present a simple template less one step synthesis of phase selective (fcc and hcp) self-supported ruthenium nanosponge using sodium borohydride and amine borane as reducing agents. Furthermore, we have addressed phase selective catalytic property of ruthenium nanosponges towards hydrogenation of benzene. Additionally, we present the catalytic efficacy of ruthenium nanosponge towards the selective hydrogenation of several other substituted arenes and aryl ethers.

[a] Dr. Sourav Ghosh, Prof. Balaji R. Jagirdar
Department of Inorganic and Physical Chemistry
Indian Institution of Science
Bangalore, Karnataka – 560012, India.
E-mail: jagirdar@ipc.iisc.ernet.in

Supporting information for this article is given via a link at the end of the document.

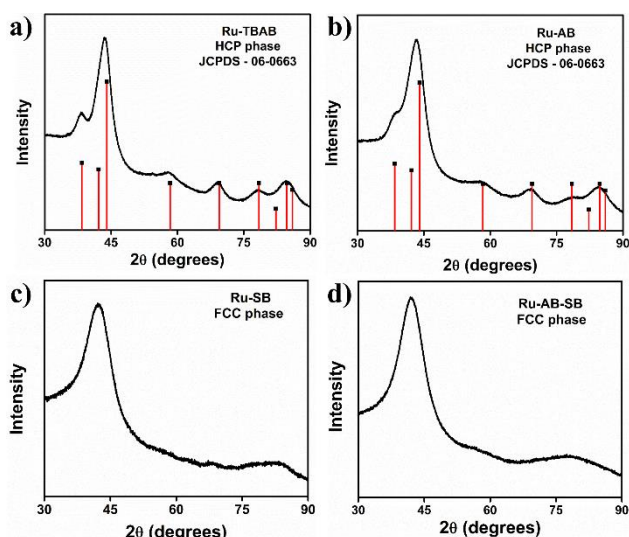


Figure 1. Powder X-ray diffraction patterns of: a) Ru-TBAB, b) Ru-AB, c) Ru-SB, and d) Ru-AB-SB nanosponges.

Results and Discussion

Synthesis and characterization of ruthenium nanosponge

Ruthenium nanoparticles were found to be catalytically active for hydrogen release via B-H bond (amine boranes and sodium borohydride) hydrolysis.^[52] This prompted us to synthesize high surface area ruthenium nanosponges using amine boranes and sodium borohydride as reducing agents. We prepared ruthenium nanosponge by reduction of ruthenium chloride in water using amine boranes and sodium borohydride in excess at room temperature. The molar ratio of ruthenium chloride to reducing agent was maintained at 5. Powder XRD patterns of Ru nanosponges obtained using various reducing agents are shown in Fig. 1. In case of amine borane (ammonia borane- AB and tert-butylamine borane- TBAB) as a reducing agent, we obtained hcp ruthenium (JCPDS – 06-0663), whereas fcc ruthenium was obtained when sodium borohydride (SB) was used as a reducing agent (Fig. 1). The broadness of the peaks is indicative of nanostructured ruthenium. In addition, when a mixture of AB and SB was used as a reducing agent, fcc ruthenium phase was obtained. The ruthenium nanosponges have been labeled as Ru-TBAB, Ru-AB, Ru-SB, and Ru-AB-SB, according to the reducing agents used for the synthesis which are TBAB, AB, SB, and a mixture of AB and SB, respectively. Earlier, hcp ruthenium nanoparticles were obtained using amine borane as a reducing agent.^[53] On the other hand, use of sodium borohydride as a reducing agent led to the formation of fcc ruthenium.^[54]

Morphological characterization was done using scanning electron microscopy (SEM). Low resolution SEM images of ruthenium nanosponges evidenced the porous nature of the samples (Fig. 2a-d). It is evident from the high-resolution SEM images (Fig. 2e-h) that these porous samples are made up of

Table 1. Surface area, pore size, and pore volume of ruthenium nanosponges

Materials (phase)	Surface area (m ² /g)	Pore size (nm)	Pore volume (cm ³ /g)
Ru-TBAB (hcp)	146.7	19.7	0.444
Ru-AB (hcp)	84.6	16.5	0.222
Ru-SB (fcc)	83	18.1	0.27
Ru-AB-SB (fcc)	67	29.1	0.312

small sized ruthenium nanoparticles. Despite the difference in the reducing power of amine boranes and sodium borohydride, in all cases formation of nanosponges was noted. Fig 3 shows the bright field TEM (BF-TEM) images of ruthenium nanosponges. The high resolution TEM images (HRTEM) (Fig. 3e-h) revealed lattice fringes with d spacing of 0.205 nm corresponding to the (101) plane of hexagonal close packed phase of Ru-AB and Ru-TBAB (Fig 3e,f). On the other hand, samples obtained using SB and AB-SB displayed lattice fringes with d spacing of 0.221 nm (Ru-SB) and 0.218 nm (Ru-AB-SB) corresponding to the (111) plane of fcc phase of ruthenium (Fig 3g-h). The selected area electron diffraction (SAED) pattern showed a ring pattern for all the samples (Fig. 3i-l). The diffraction ring pattern in case of Ru-TBAB and Ru-AB could be indexed to the hcp phase of ruthenium (Fig 3i-j) and, the fcc phase of ruthenium in case of Ru-SB and Ru-AB-SB samples respectively (Fig 3k-l).

The EDS spectra showed the presence of Ru(0) only (see supporting information, SI). The featureless FT-IR spectrum further supports that ruthenium nanosponge is comprised of only ruthenium metal (SI). The deconvoluted 3d core level XPS spectrum of ruthenium (Ru-TBAB) consists of four peaks having binding energies of 280.1 eV (3d_{5/2}) and 284.3 eV (3d_{3/2}) which correspond to Ru (0) and two other peaks (280.7 eV - 3d_{5/2}; 285.2 eV - 3d_{3/2}) which could be ascribed to ruthenium oxide (see SI).^[55] Similarly, XPS spectra were recorded for the other ruthenium nanosponges (see SI) and the binding energy values for different oxidation states of various ruthenium samples have been summarized in the SI. Formation of ruthenium oxide is unavoidable, since the samples were stored under ambient conditions and all the manipulations were carried out in aerial conditions. Presence of Ru(0) and Ru(IV) were further verified from the core level spectra of 3p states and the results have been tabulated in the SI. The nitrogen adsorption and desorption isotherms measured at 77 K (see SI), evidence their type IV nature (more specifically, H3 type); hysteresis was noted for all the isotherms which is indicative of mesoporosity.^[56] The BET surface area, pore size, and pore volume values for all the nanosponges have been tabulated in Table 1. It was found that, Ru-TBAB nanosponge possessed the highest surface area, followed by Ru-AB, Ru-SB and Ru-AB-SB nanosponges.

To evaluate the effect of reducing agents on the porosity of ruthenium nanosponges, we measured the hydrogen evolution rates during the reduction reaction using different

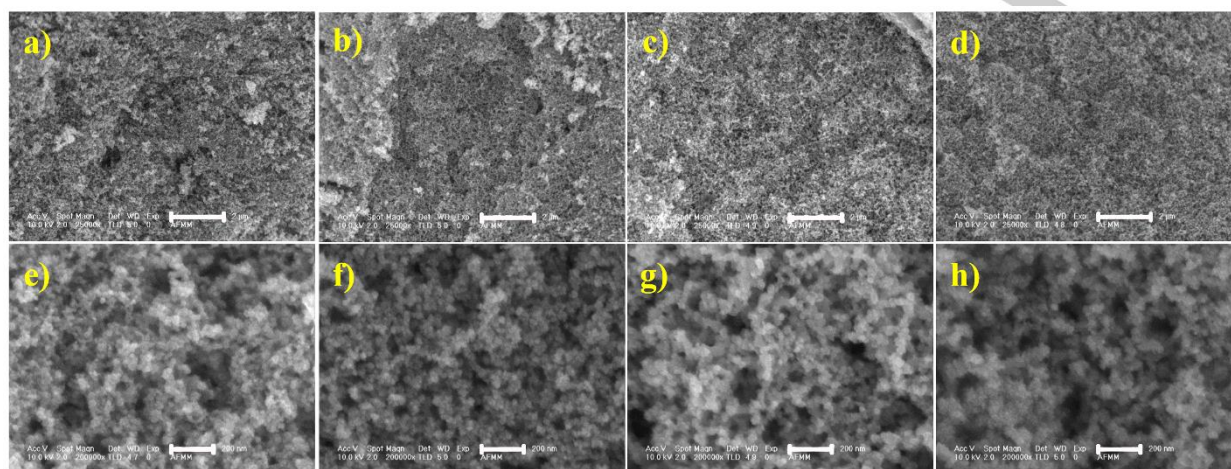


Figure 2. Ru-TBAB, Ru-AB, Ru-SB, Ru-AB-SB nanosponges: a-d) low resolution SEM images (scale bar- 2 μ m); e-h) high resolution SEM images (scale bar- 200 nm).

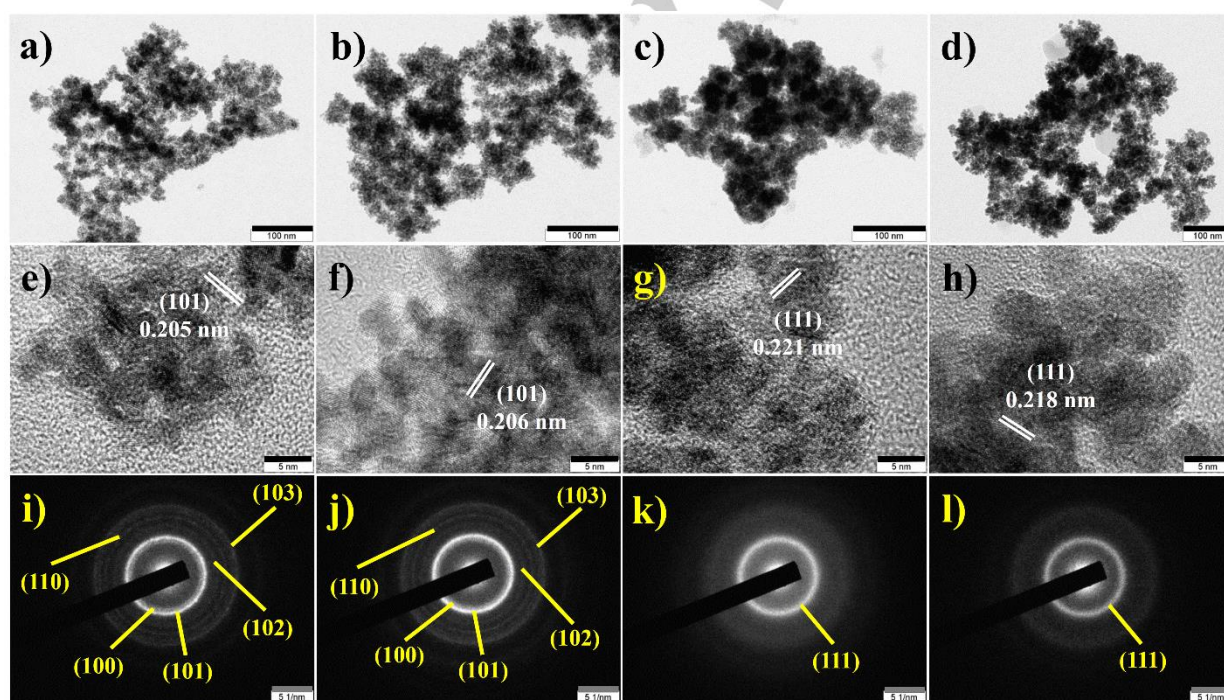


Figure 3. Ru-TBAB, Ru-AB, Ru-SB, Ru-AB-SB nanosponges: a-d) BF-TEM images (scale bar- 100 nm); e-h) HRTEM images (scale bar- 5 nm); i-l) SAED patterns (scale bar- 5 1/nm).

reducing agents (sodium borohydride and amine boranes). We found that the hydrolysis rates were slower when amine boranes (ammonia borane, tertiary butylamine borane) were used as reducing agents as compared to, when sodium borohydride was used (see S.I.). The faster reduction kinetics of sodium borohydride led to the formation of irregularly shaped ruthenium

nanoparticles which eventually resulted in a low surface area ruthenium nanosponge with metastable fcc phase. On the other hand, amine borane derivatives reduced the ruthenium salt at a slower rate leading to the formation of high surface area ruthenium nanosponge with stable hcp phase.

Catalytic activity of different phases of ruthenium

Table 2. Hydrogenation of benzene using ruthenium catalysts at different substrate to catalyst molar ratio

Entry	Catalyst (phase)	S/C ratio	Time (h)	%Conv ^c	TOF _i (h ⁻¹) ^d
1	Ru-TBAB(<i>hcp</i>)	1000	15	60	176
2	Ru-AB(<i>hcp</i>)	1000	15	50	60
3	Ru-SB(<i>fcc</i>)	1000	15	15	52
4	Ru-AB-SB(<i>fcc</i>)	1000	15	15	48
5	Ru-TBAB(<i>hcp</i>)	500	4.5	>99	187
6	Ru-AB(<i>hcp</i>)	500	5	>99	106
7	Ru-SB(<i>fcc</i>)	500	11	95	102
8	Ru-AB-SB(<i>fcc</i>)	500	8.5	90	103
9	Ru-TBAB(<i>hcp</i>)	250	1.33	>99	252
10	Ru-AB(<i>hcp</i>)	250	1.5	>99	185
11	Ru-SB(<i>fcc</i>)	250	2.75	>99	103
12	Ru-AB-SB(<i>fcc</i>)	250	2.5	>99	111
13	Ru-TBAB(<i>hcp</i>)	250	0.58	>99	614
14	Ru-AB(<i>hcp</i>)	250	1.25	>99	348
15	Ru-SB(<i>fcc</i>)	250	6.5	>99	72
16	Ru-AB-SB(<i>fcc</i>)	250	6.75	>99	75

^aEntry 1-12: all reactions were carried out at a constant temperature of 75 °C and 4 bar hydrogen gas pressure and neat benzene was used; ^bentries 13-16: all reactions were carried out in 10 mL of n-heptane as a solvent (ruthenium nanosponge (16.2 mg, 0.16 mmol) and benzene (3.56 mL, 40 mmol)), at a constant temperature of 75 °C and 4 bar hydrogen gas pressure; ^cconversion determined by GC/MS analysis; ^dinitial turnover frequency (TOF) = mol(benzene)/mol(Ru nanosponge)·0.25, after 15 min (0.25 h).

The catalytic activities of as prepared fcc and hcp ruthenium nanosponges were investigated using benzene hydrogenation as a model reaction. All the catalysts were found to be active towards hydrogenation of benzene to cyclohexane under moderate conditions (at 75 °C and 4 bar). Blank runs in the absence of ruthenium catalysts under similar conditions did not result in hydrogenation. Separation of the catalysts from the reaction mixture was achieved by simple centrifugation followed by decantation. The catalytic activity of different ruthenium catalysts was probed by carrying out hydrogenation of benzene at different substrate to catalyst ratios either in the neat condition (without any solvent) or in n-heptane as a solvent. Results of these studies have been summarized in Table 2. In all these cases, cyclohexane was obtained as a product; no partial hydrogenation product (cyclohexene) was noted. In case of substrate to catalyst ratio of 1000, incomplete conversion of benzene to cyclohexane was noted for the two phases of

ruthenium catalysts. Upon decreasing the substrate to catalyst ratio from 1000 to 250, complete conversion of benzene to cyclohexane was noted using both hcp and fcc ruthenium catalysts and turnover frequency (TOF) value increased. For substrate to catalyst ratio of 250, highest TOF values were noted as compared to other substrate to catalyst ratios. In all these cases, it was found that the catalytic activity depends on the crystallographic phase of ruthenium: hcp ruthenium is more active than fcc ruthenium. Similarly, when benzene hydrogenation was carried out using different ruthenium catalysts with a fixed substrate to catalyst ratio of 250 in n-heptane as a solvent instead of neat benzene, better catalytic activity for hcp ruthenium was noted as compared to fcc ruthenium. At this stage, the origin of the phase selectivity towards catalysis is not clear. But we propose that, the benzene molecules get adsorbed more strongly onto the hcp phase of ruthenium as compared to the fcc phase. On the other hand, both adsorption and desorption of benzene takes place on the surface of fcc phase at a rapid rate, is reflected in a lower hydrogenation catalytic activity in this case in comparison to that of the hcp phase. More work will be needed to decipher the intricate mechanistic aspects involved in this phase selective hydrogenation activity. Since these are heterogeneous catalysts and the catalytic processes take place at the surface of the materials, the difference in surface area could play an important role for defining catalytic activities. Among different hcp ruthenium catalysts (Ru-TBAB and Ru-AB), high surface area Ru-TBAB shows greater activity towards catalytic hydrogenation reaction as compared to the low surface area Ru-AB (see SI).

Thermal stability of ruthenium nanosponge: Thermal stability of the catalysts was studied by annealing them at different temperatures under inert atmosphere. Catalysts annealed at 150 °C for 3 h were labeled as Ru-TBAB-150, Ru-AB-150, Ru-SB-150, Ru-AB-SB-150 and the catalysts annealed at 300 °C for 3 h were labeled as Ru-TBAB-300, Ru-AB-300, Ru-SB-300, Ru-AB-SB-300. Morphological characterization of the annealed samples

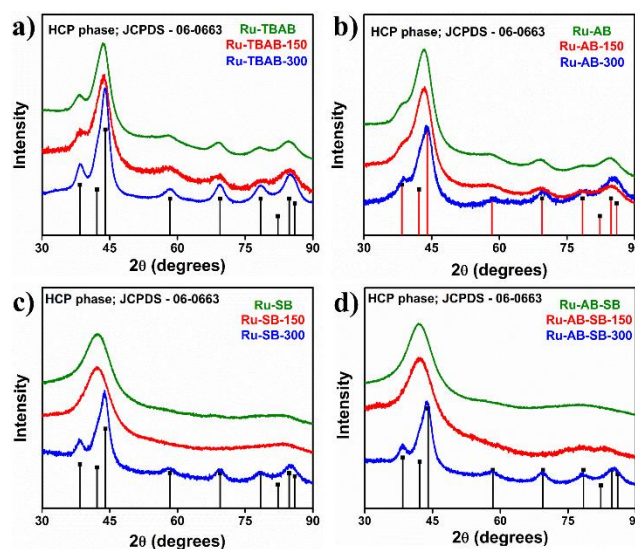


Figure 4. Powder XRD pattern stack plots of ruthenium nanosponges before and after annealing (150 °C and 300 °C): a) Ru-TBAB, b) Ru-AB, c) Ru-SB, and d) Ru-AB-SB.

Table 3. Surface area and pore size of ruthenium nanosponges before and after annealing

Entry	Catalyst (phase)	Surface area (m ² /g)	Pore size (nm)
1	Ru-TBAB (hcp)	146.7	19.7
2	Ru-TBAB-150 (hcp)	138.9	31.5
3	Ru-TBAB-300 (hcp)	105	21.7
4	Ru-AB (hcp)	84.6	16.5
5	Ru-AB-150 (hcp)	77.7	20.8
6	Ru-AB-300 (hcp)	62.6	14.9
7	Ru-SB (fcc)	83	18.2
8	Ru-SB-150 (fcc)	72.1	22.5
9	Ru-SB-300 (hcp)	39.6	27
10	Ru-AB-SB (fcc)	67	29.1
11	Ru-AB-SB-150 (fcc)	57.8	40.7
12	Ru-AB-SB-300 (hcp)	35.7	36.9

Table 4. Hydrogenation of benzene using as prepared and annealed ruthenium nanosponges

Entry	Catalyst	Phase	Time (h)	%Conv ^b	TOF(h ⁻¹) ^c
1	Ru-TBAB	hcp	0.58	>99	431
2	Ru-TBAB-150	hcp	0.58	>99	431
3	Ru-TBAB-300	hcp	0.58	90	388
4	Ru-AB	hcp	1.25	>99	200
5	Ru-AB-150	hcp	1.25	99	198
6	Ru-AB-300	hcp	1.25	88	176
7	Ru-SB	fcc	6.5	>99	38.5
8	Ru-SB-150	fcc	6.5	85	32.7
9	Ru-SB-300	hcp	6.5	50	19.2
10	Ru-AB-SB	fcc	6.75	>99	37
11	Ru-AB-SB-150	fcc	6.75	80	29.6
12	Ru-AB-SB-300	hcp	6.75	44	16.3

^aAll reactions were carried out at a constant temperature of 75 °C and 4 bar pressure in 10 mL of n-heptane at 250 benzene/catalyst molar ratio (40 mmol

of benzene, 0.16 mmol of Ru catalyst); ^bconversion determined by GC-MS analysis; ^cturnover frequency = mol(benzene)/mol(Ru nanosponge)·h.

using SEM (see SI) revealed no changes as compared to un-annealed samples. Additionally, powder XRD patterns revealed that both Ru-TBAB and Ru-AB samples retained their hcp phase even upon annealing at 150 °C and 300 °C (Fig. 4a-b). The fcc phases of Ru-SB and Ru-AB-SB were also retained for samples annealed at 150 °C, but a phase change from fcc to hcp was noted when these samples were annealed at 300 °C (Fig. 4c-d). It was reported that the fcc phase of ruthenium is a metastable phase and has not been observed in the bulk, whereas, hcp is the bulk phase of ruthenium.^[54,57] Hence, a phase change was expected to take place at high temperature. High temperature annealing resulted in sintering of particles which was reflected by a decrease in their surface areas (Table 3). Interestingly, in case of samples exhibiting fcc phase (Ru-SB and Ru-AB-SB), the magnitude of change in surface area was found to be greater than that in case of hcp phase (Ru-TBAB and Ru-AB). This could be ascribed to a thermal induced phase change (fcc to hcp) which could lead to a structural reorganization resulting in a considerable change in surface area.

Catalytic activities of the annealed samples were assessed using benzene hydrogenation as a model reaction. Table 4 summarizes the results of these studies. In case of hcp ruthenium catalysts (Ru-TBAB and Ru-AB), TOF values remained constant for samples annealed at 150 °C whereas, 90% of benzene was converted into cyclohexane for samples annealed at 300 °C. Similarly, fcc samples annealed at 150 °C brought about hydrogenation to an extent of 80% using Ru-AB-SB-150 and 85% using Ru-SB-150 catalysts. On the other hand, fcc samples annealed at 300 °C (which got transformed to hcp phase) brought about hydrogenation to an extent of 44% using Ru-AB-SB-300 and 50% using Ru-SB-300 catalysts. These variations in catalytic activities could be ascribed to the different extent of reduction in surface area for the different phases of ruthenium nanosponges upon annealing. Thermal annealing study and substrate to catalyst ratio optimization study show that the Ru-TBAB (hcp phase) is the most active catalyst among various ruthenium nanosponges. Thus, the optimum conditions required for benzene hydrogenation was investigated using Ru-TBAB as a catalyst by a careful change in pressure, temperature, and solvent.

Effect of temperature, pressure, and solvent on catalytic activity of ruthenium (Ru-TBAB) catalyst: Data for benzene hydrogenation catalysis using Ru-TBAB catalyst are summarized in the SI. As it is evident from the data, complete benzene hydrogenation required shorter times when the reaction was carried out at high temperatures. At room temperature and 4 bar of hydrogen pressure, 95% benzene was hydrogenated to cyclohexane after 11 h whereas, >99% conversion was noted at 75 °C within 35 min. The TOF was calculated to be 431 h⁻¹ (75 °C, 4 bar) which is comparable to the literature report for benzene hydrogenation using ruthenium nanoparticles under moderate conditions.^[22,58-61] In another set of experiments, benzene hydrogenation was carried out at different hydrogen gas pressures by keeping all the other parameters constant (0.4 mol% catalyst, 40 mmol substrate in 10 mL of n-heptane at 75

°C). It is also apparent that an increase in pressure leads to an increase in the rate of hydrogenation. No saturation of TOF was noted up to a pressure of 6 bar.

Hydrogenation of benzene was carried out in different solvents and the results are summarized in the SI. It was noted that solvent polarity does not influence the catalytic activity. However, higher rate of hydrogenation was noted for solvents

Table 5. Hydrogenation of substituted arenes using hcp Ru-TBAB nanosponge

Entry	Substrate	Time (h)	Product	TOF(h ⁻¹) ^a
1	Benzene	0.58	Cyclohexane	431
2	Toluene	0.66	Methylcyclohexane	378.8
3	Ethylbenzene	1.25	Ethylcyclohexane	200
4	Isopropylbenzene	2	Isopropylcyclohexane	125
5	t-Butylbenzene	3	t-Butylcyclohexane	83.3
6	Styrene	2	Ethylcyclohexane	125
7	<i>o</i> -Xylene	11	1,2-Dimethylcyclohexane	22.7
8	<i>m</i> -Xylene	8	1,3-Dimethylcyclohexane	31.3
9	<i>p</i> -Xylene	5.5	1,4-Dimethylcyclohexane	45.5
10	Mesitylene	15	1,3,5-Trimethylcyclohexane	16.7
11	Biphenyl	20	Bicyclohexane	12.5

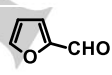
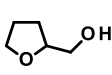
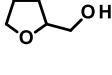
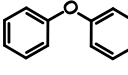
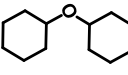
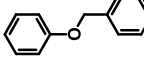
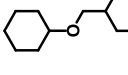
All reactions were carried out at a constant temperature of 75 °C and 4 bar hydrogen gas pressure in 10 mL of n-heptane as a solvent at 250 substrate/Ru-TBAB molar ratio (40 mmol of substrate, 0.16 mmol of Ru-TBAB catalyst); in each case >99 % substrate to product conversion was determined by GC-MS analysis; ^aturnover frequency = mol(substrate)/mol(Ru nanosponge)-h.

which have good hydrogen solubility.^[62] In case of cyclohexane, hydrogen solubility decreases with increasing the temperature which in turn causes a drop in TOF.^[63] No appreciable hydrogenation activity was noted in acetonitrile due to a competitive adsorption of the substrate and the solvent on the catalyst surface. Moderate activity was noted in alcohol and water as solvents.

Hydrogenation of substituted arenes and aryl ethers using Ru-TBAB catalyst: To understand the scope of the Ru-TBAB catalyst, various alkylated benzenes were hydrogenated under relatively mild conditions (75 °C and 4 bar, n-heptane). Results are summarized in Table 5. In all the cases, >99% conversion of substituted arene to substituted cyclohexane was noted. The TOF value decreases with an increase in the steric bulkiness of the substituent on benzene (TOF_{toluene} = 378.8 h⁻¹ > TOF_{ethylbenzene} = 200 h⁻¹ > TOF_{isopropylbenzene} = 125 h⁻¹ > TOF_{t-butylbenzene} = 83.3 h⁻¹). Similarly, upon increasing the number of

methyl groups, steric bulkiness of the substrate increases and subsequently the hydrogenation rate slowed down which is reflected in the TOF values (TOF_{benzene} > TOF_{xylene} > TOF_{mesitylene}). In case of hydrogenation of xylene, the cis product was obtained in higher amount compared to the trans isomer. We also found that, Ru-TBAB is capable of hydrogenating biphenyl to bicyclohexane (an important organic hydrogen storage medium) with a TOF of 12.5 h⁻¹ (TON = 250).^[64]

Table 6. Hydrogenation of substituted benzenes (phenol, aryl ether, aryl ketone) using hcp Ru-TBAB nanosponge

Entry	Substrate	Time (h)	%Conv. (%Selec.) ^a	Product
1		4	>99(99)	
2		3	>99(99)	
3		4	>99(99)	
4		4	>99(98)	
5		4	>99(99)	
6		12	>99(93)	
7		24	>99(45) ^b	
8		24 ^c 24 ^d 10 ^e 6 ^f	7(1) ^c 91(74) ^d >99(87) ^e >99(88) ^f	
9		10	>99(99)	

All reactions were carried out at a constant temperature of 75 °C and 20 bar hydrogen gas pressure in 3 mL of n-heptane as a solvent at 133 substrate/Ru-TBAB molar ratio (4 mmol of substrate, 0.03 mmol of Ru-TBAB catalyst);

^aproduct conversion was determined by GC-MS analysis; ^b>99% conversion of benzaldehyde was observed and 45% cyclohexylmethanol and 44% benzyl alcohol was obtained; ^cdiphenyl ether:Ru (250), 5 Bar H₂/75 °C; ^ddiphenyl

ether:Ru (250), 20 Bar H₂/75 °C; ^ediphenyl ether:Ru (133), 20 Bar H₂/75 °C; ^fdiphenyl ether:Ru (100), 20 Bar H₂/75 °C.

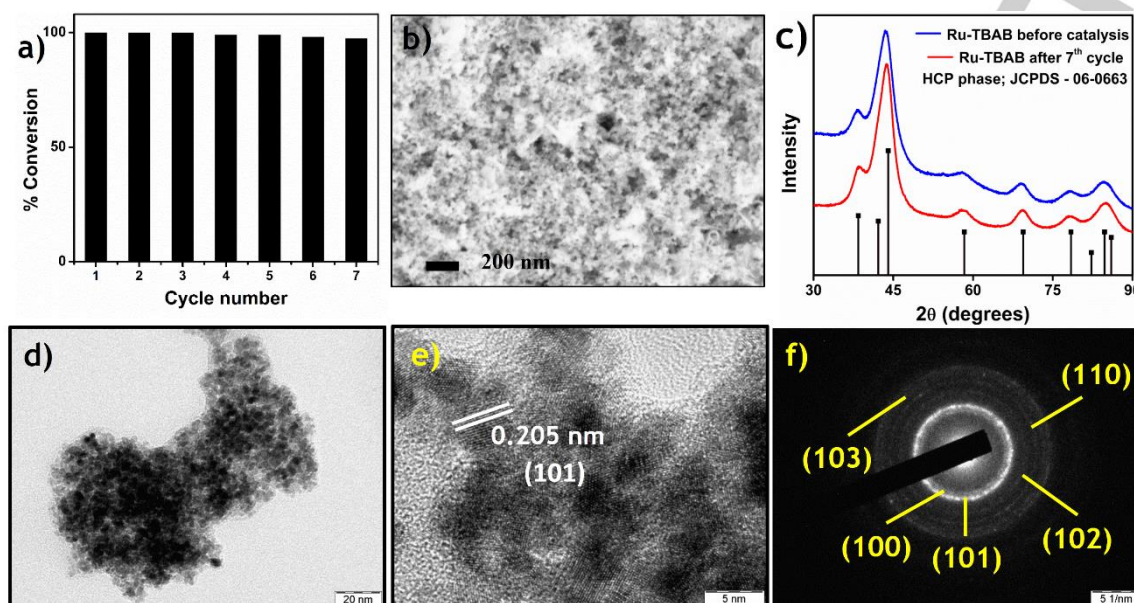
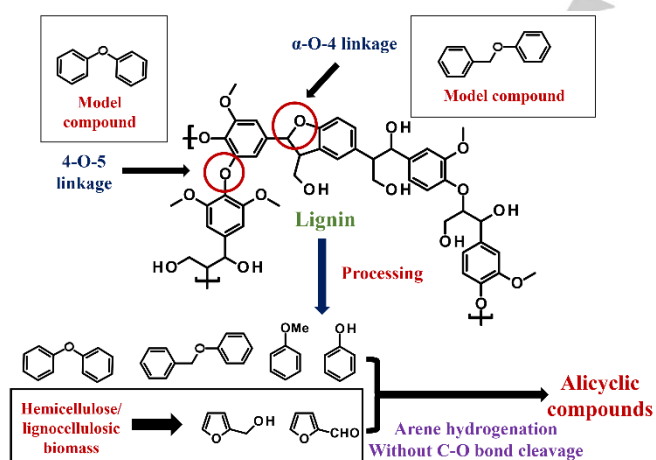


Figure 5. a) Catalyst activity for benzene hydrogenation by ruthenium nanosponge in n-heptane upon recycling, b) SEM image, c) powder XRD stack plot of Ru-TBAB before and after catalysis, d) BF-TEM image, e) HRTEM image, and f) SAED pattern of the ruthenium catalyst after 7 cycles of hydrogenation.



Scheme 1. Fragments derived from lignin and cellulosic biomass.

A clear majority of the industrially important arene derivatives are produced from fossil fuel feedstock. However the rapid depletion of fossil fuels necessitates a search for sustainable alternatives such as biomass (lignin, cellulose, hemicellulose) whose valorization produces oxygenated aromatics.^[65-67] For subsequent utilization of such oxygenated aromatics, several transition metal based homogeneous and heterogeneous catalysts have been developed which afford mainly C–O bond hydrogenolysis products.^[68-71] On the other

hand, selective hydrogenation of aromatic cores of lignin derived compounds and other oxygenated aromatics are also important chemical transformations for the generation of alicyclic ethers, which are key intermediates for the production of bio-fuels and fine chemicals (Scheme 1).^[72] Reports of these transformations are rather scarce.^[72] In this context, the catalytic ability of Ru-TBAB was further assessed by carrying out the hydrogenation of phenol at 75 °C and 4 bar which gave a poor yield of cyclohexanol. Upon increasing the pressure to 20 bar, nearly quantitative conversion to cyclohexanol without C–O bond hydrogenolysis was noted (Table 6, entry 1). Subsequently, the hydrogenation of anisole resulted in the formation of methoxycyclohexane (Table 6, entry 2). In case of acetophenone, complete reduction of both arene and ketone moieties was noted. Similarly, selective conversion of furfural and furfuryl alcohol to the corresponding tetrahydrofurfural was achieved; tetrahydrofurfural is an industrially important compound. In general, benzylic compounds (benzyl ethers and benzyl alcohols) are quite prone to hydrogenolysis during hydrogenation because of their low C–O bond dissociation energy.^[73] Herein, hydrogenation of benzyl alcohol proceeded efficiently to the corresponding saturated alicyclic alcohol with 93% selectivity (Table 6, entry 6). Similarly, hydrogenation of benzaldehyde resulted in the formation of benzyl alcohol followed by 45 % conversion into the saturated alicyclic alcohol was noted. In case of diphenyl ether, the optimum hydrogenation conditions were achieved by carefully varying the substrate to catalyst ratio and hydrogen gas pressure. In case of

0.75 mol% catalyst loading at 20 bar pressure after 10 h, dicyclohexyl ether was obtained with 87% selectivity and 13% C–O bond hydrogenolysis products. Similarly, hydrogenation of phenyl benzyl ether resulted in the formation of alicyclic ether with 99% selectivity (>99% conversion). All these results clearly suggest that hcp ruthenium is solely responsible for the catalytic hydrogenation of aromatic ring over the C–O bond cleavage.

Catalyst recyclability and catalyst poisoning: Catalyst recyclability was evaluated for Ru-TBAB catalysts using benzene hydrogenation under similar conditions as mentioned above: 0.4 mol% catalyst, 40 mmol substrate in 10 mL of n-heptane at 75 °C. Figure 5a shows the percentage conversion over 7 cycles. Even after the 7th cycle, the catalyst is still active and capable of hydrogenating ~97% benzene to cyclohexane. The SEM images confirm that the spongy nature of the catalyst remained unaltered (Fig. 5b). Additionally, powder XRD pattern showed no structural change (Fig. 5c). Further, BF-TEM image of recycled ruthenium nanosponge revealed that the porous nature of the samples remained intact (Fig. 5d). Moreover, the HRTEM image exhibited lattice fringes with d spacing of 0.205 nm corresponding to the (101) lattice plane of hcp ruthenium (Fig. 5e). The SAED pattern could be perfectly indexed to the hcp phase of ruthenium (Fig. 5f). The mesoporous nature of the catalyst is responsible for its long-term stability and high catalytic activity. Thus, it is evident that the catalyst is robust and retains its morphology and activity for several cycles. Hot filtration study was carried out to illustrate the true heterogeneous nature of the catalyst and to rule out the possibility of catalyst leaching. After about 50% conversion of benzene using the Ru-TBAB catalyst, the hot reaction mixture was passed through a hot (~75 °C) frit and the supernatant was again subjected to hydrogenation under similar reaction conditions (75 °C and 4 bar). No further hydrogenation of benzene took place which demonstrates the heterogeneous nature of the catalyst. Catalyst poisoning experiments were performed using PCy₃, a well-known catalyst poison.^[30] Hydrogenation of benzene using Ru-TBAB in presence of PCy₃ in 1:5 molar ratio (catalyst: poison) at 75 °C in n-heptane showed no catalytic activity even after 2 h of reaction. Similarly, poisoning experiment was carried out by addition of 5 equiv. of PCy₃ after about 50% conversion which resulted in an instantaneous suppression of catalytic activity. In this case, strong binding of PCy₃ on the catalyst surface blocks the catalytically active sites. Additionally, carbon monoxide^[74] and thiophene^[75] were used separately as catalyst poisons, wherein suppression of catalytic activity was noted for carbon monoxide and thiophene treated catalyst (Ru-TBAB). Since, ruthenium nanosponge exhibits good catalytic activity towards arene hydrogenation, it would be important to study the effect of alloying with other metals to understand the catalytic activity at moderate reaction conditions with lower catalyst loading. Research in this direction are currently being pursued in our laboratories.

Conclusions

In summary, phase selective ruthenium nanosponge was synthesized by chemical reduction method using amine borane and sodium borohydride as a reducing agent. These nanosponges were utilized as a catalyst for benzene hydrogenation reaction wherein, hcp ruthenium shows better catalytic activity as compared to the fcc ruthenium. Among the two different hcp ruthenium catalysts, Ru-TBAB showed better catalytic activity as compared to the Ru-AB due to its high surface area. Thermal annealing study showed that the hcp phase of ruthenium is thermally more stable and active than the fcc phase. On the other hand, fcc phase undergoes a thermally induced phase transition to hcp ruthenium which is associated with substantial change in the surface area and the catalytic activity. Using Ru-TBAB as a catalyst, several other substituted benzenes were successfully hydrogenated under mild conditions. Furthermore, the aromatic moieties of phenol and aryl ethers were selectively hydrogenated using Ru-TBAB nanosponge to their alicyclic components without C–O bond hydrogenolysis. The catalytic activity of these nanosponge catalysts opens new opportunities for the valorization of lignin derived aromatic compounds under mild conditions in a green and sustainable manner. Hence in future, the catalytic activity of these metal nanosponges could further be tuned for efficient and sustainable transformation of biomass feedstock to valuable chemicals under moderate conditions.

Experimental Section

Materials

Ruthenium chloride (RuCl₃.xH₂O) was purchased from Arora Matthey Limited, India. Sodium borohydride (NaBH₄), ammonium sulfate ((NH₄)₂SO₄), n-heptane, thiophene, and tetrahydrofuran (THF) were purchased from S. D. Fine Chemicals Limited, India. Tert-butylamine borane (TBAB) and tricyclohexylphosphine (PCy₃) were procured from Sigma Aldrich. All the arenes were used as received. THF and n-heptane were dried over Na-benzophenone. Ammonia borane was synthesized following literature procedure and characterized using ¹¹B NMR and FT-IR spectroscopy before use.^[76] Double distilled water was used for all the reactions.

Synthesis of ruthenium nanosponge

Ruthenium nanosponge was prepared by adopting a literature procedure using NaBH₄, AB (H₃N-BH₃), and TBAB (^tBuH₂N-BH₃) as reducing agents.^[49] In a typical experiment, 310 mg (10 mmol) of AB was dissolved in 100 mL of water in a 500 mL round bottomed flask. Ruthenium chloride, RuCl₃.xH₂O (415 mg, 2 mmol) was dissolved in 20 mL of water and added to the aqueous solution of AB under vigorous stirring. Strong effervescence of hydrogen gas was noted. After 5 min, the black residue was filtered and washed thoroughly with water and acetone and kept for drying overnight. The yield obtained was 148 mg (73.2 %). The ruthenium nanosponge was labelled as Ru-AB. In a similar manner, sodium borohydride (NaBH₄, SB) (378.3 mg, 10 mmol) and RuCl₃.xH₂O (415 mg, 2 mmol) were allowed to react in water following the above procedure and the nanosponge obtained was labelled as Ru-SB. The yield obtained was 156 mg (77.2 %). Similarly, tert-butylamine borane (^tBuH₂N-BH₃, TBAB) (869.7 mg, 10 mmol) and RuCl₃.xH₂O (415 mg, 2 mmol) were reacted in water to obtain the Ru-TBAB nanosponge.

The yield obtained was 155 mg (76.7 %). Ruthenium nanosponge was also synthesized using a mixture of AB (155 mg, 5 mmol) and SB (189 mg, 5 mmol) from $\text{RuCl}_3 \cdot x\text{H}_2\text{O}$ (415 mg, 2 mmol) in water and the catalyst was labelled as Ru-AB-SB. The yield obtained was 160 mg (79.1 %).

Characterization

Scanning electron microscopy (SEM) images were acquired using FEI Sirion XL₃₀ FEG SEM. Powder samples were placed on a double-sided conductive carbon tape supported on an aluminum stub. Powder XRD patterns were acquired using PANalytical EMPYREAN diffractometer using Cu K α radiation. Bright field (BF) TEM imaging, high resolution (HR) TEM imaging, and selected area electron diffraction (SAED) experiments were performed using a JEOL 2100F FETEM. Energy dispersive X-ray spectroscopy (EDS) was performed using Oxford EDS spectrometer attached to the TEM. The operating voltage of the field emission gun (FEG) is 200 kV. Samples were prepared by dispersing 2 mg of ruthenium sponge in 4 mL of THF and 5 μL solutions were drop casted on a 300 mesh formvar coated copper grid and dried under a 40 Watt lamp for 12 h. FT-IR spectra were recorded using Bruker ALPHA FTIR spectrometer. X-ray photoelectron spectroscopy was carried out using a Kratos AXIS Ultra XPS spectrometer. BET surface area and porosity measurements were performed using Micromeritics ASAP 2020. NMR spectral measurements were carried out using an Avance Bruker 400 MHz spectrometer.

General procedure for hydrogenation catalysis

Ultra-high purity (99.997%) hydrogen gas was obtained from Bhuruka Gases Limited, India. All the hydrogenation experiments were carried out in n-heptane solvent using a Parr hydrogenation apparatus. In a typical experiment, ruthenium nanosponge (16.2 mg, 0.16 mmol) was dispersed in 10 mL of n-heptane and then 3.56 mL (40 mmol) of benzene was added to the reaction mixture. The mixture was sonicated for 3 min and then placed in a Parr hydrogenation apparatus and closed with a neoprene stopper. Before starting the reaction, an aliquot was drawn for recording ^1H NMR spectrum. The bottle was pressurized with 3 bar of hydrogen and then depressurized for four times before each catalysis experiment. Temperature was fixed at 75 °C and the bottle was pressurized with 4 bar of H_2 . The reaction was monitored until gas consumption ceased which was evident from no further pressure drop. The reaction mixture was cooled down and centrifuged to separate the filtrate from the catalyst. The filtrate was characterized using GC-MS and ^1H -NMR spectroscopy. Same procedure was followed for hydrogenation of the remaining substrates in n-heptane.

Samples of the reaction mixture were withdrawn and analyzed by using Shimadzu GCMS-QP2010 SE gas chromatograph-mass spectrometer, installed with an Rtx-5MS capillary column (0.25mm x 30m x 0.25 μm) and a high-performance quadrupole mass detector. Each reaction was performed twice for reproducibility and the mass spectra of the products were matched with the NIST library. The percentage conversion was calculated based on peak areas, with respect to the n-dodecane as an internal standard.

General procedure for hydrogenation reaction using Parr reactor

Hydrogenation of model lignin compounds and few of the substituted benzenes were performed in a stainless steel (T316) autoclave using a Parr 4590 series high pressure micro-reactor set-up. In a typical experiment, ruthenium nanosponge (3 mg, 0.03 mmol) was dispersed in 3 mL of n-heptane and then 4 mmol of substrate (diphenyl ether, 0.65 mL,

4 mmol) was added to the reaction mixture. The mixture was sonicated for 3 min and then placed in an autoclave and sealed. Subsequently, the reaction vessel was purged with hydrogen gas for 4 times; then, the solution temperature was raised to 75 °C and pressurized with 20 bar of hydrogen gas. The pressure drop was monitored until gas consumption ceased. After completion of the reaction, reaction vessel was cooled down and depressurized carefully. Finally, an aliquot was drawn for GC-MS analysis. Same procedure was followed for hydrogenation of the remaining substrates in n-heptane.

Thermal stability of the ruthenium catalysts

Thermal stability of the ruthenium catalyst was evaluated by annealing the samples in argon filled ampoules and subsequently used for benzene hydrogenation reactions. Annealing study was performed for Ru-TBAB, Ru-AB, Ru-SB, Ru-AB-SB catalysts. The ampoules were placed separately in a box furnace at 150 °C for 3 h and 300 °C for 3 h. The samples annealed at 150 °C were labelled as Ru-TBAB-150, Ru-AB-150, Ru-SB-150, and Ru-AB-SB-150. Similarly, samples annealed at 300 °C were labelled as Ru-TBAB-300, Ru-AB-300, Ru-SB-300, and Ru-AB-SB-300. Hydrogenation reactions were performed with these annealed samples at 75 °C and 4 bar H_2 pressure in n-heptane as a solvent. The reaction was carried out as described above.

Catalyst recyclability

Ruthenium nanosponge (16.2 mg, 16 mmol) was dispersed in 10 mL of n-heptane; then benzene (3.56 mL, 40 mmol) was added to the dispersion. The reaction was carried out as described above. After one cycle, the catalyst was separated by centrifugation. The filtrate was characterized using ^1H NMR spectroscopy. The catalyst was washed thoroughly with n-heptane. Then, 10 mL of n-heptane was added to the reactor and the catalyst was dispersed; subsequently, 3.56 mL of benzene was added and the next cycle was carried out for 35 min. After 7 cycles of hydrogenation, the catalyst was separated by centrifugation and washed thoroughly with n-heptane and acetone and dried for 12 h. The catalyst was characterized using powder XRD, SEM, and TEM.

Acknowledgements

The authors gratefully acknowledge the financial support from the Council of Scientific & Industrial Research (CSIR), India and the Indian Institute of Science for funding the procurement of a 200 kV FETEM. Authors thank Prof. S. Ramakrishnan of IPC department, IISc, for providing the GC-MS facility and Dr. Subhadip Chakraborty and Mr. Sujoy Bej for their help with the GC-MS measurements and Ms. Debdyuti Mukherjee for her help with the electrochemical measurement.

Keywords: Heterogeneous catalyst • Ruthenium nanosponge • HCP and FCC Phase • Arene hydrogenation • Aryl ether hydrogenation

- [1] R. L. Augustine, *Heterogeneous Catalysis for the Synthetic Chemist*, Marcel Dekker, New York, **1995**.
- [2] J. X. Liu, W. X. Li, *WIREs Comput. Mol. Sci.* **2016**, *6*(5), 571–583.
- [3] J. X. Liu, P. Wang, W. Xu, E. J. M. Hensen, *Engineering* **2017**, *3*, 467–476.
- [4] J. X. Liu, H. Y. Su, D. P. Sun, B. Y. Zhang, W. X. Li, *J. Am. Chem. Soc.* **2013**, *135*, 16284–16287.

- [5] Z. Fan, Z. Hua, *Acc. Chem. Res.* **2016**, *49* (12), 2841–2850.
- [6] P. Sabatier, *Ind. Eng. Chem.* **1926**, *18*, 1005–1008.
- [7] P. Sabatier, J. B. Senderens, *C. R. Hebd. Sciences Acad. Sci.* **1901**, *132*, 210–212.
- [8] D. S. Wang, Q. Chen, S. M. Lu, Y. G. Zhou, *Chem. Rev.* **2012**, *112*, 2557–2590.
- [9] J. A. Widegren, R. G. Finke, *J. Mol. Catal. A: Chem.* **2003**, *191*, 187–207.
- [10] G. C. Bond, *Hydrogenation of the Aromatic Ring. In: Metal-Catalysed Reactions of Hydrocarbons. Fundamental and Applied Catalysis*, Springer, Boston, MA, **2005**, pp. 437–471.
- [11] T. J. Donohoe, R. Garg, C. A. Stevenson, *Tetrahedron: Asymmetry* **1996**, *7*, 317–344.
- [12] K. Weissert, H. J. Arpe, *Industrial Organic Chemistry*, VCH, New York, **1993**.
- [13] G. W. Parshall, S. D. Ittel, *The applications and chemistry of catalysis by soluble transition metal complexes, in: Homogeneous Catalysis*, Wiley, New York, **1992**.
- [14] P. N. Rylander, *Catalytic Hydrogenation in Organic Synthesis*, Academic Press, New York, **1979**.
- [15] A. Corma, A. Martínez, V. Martínez-Soria, *J. Catal.* **1997**, *169*, 480–489.
- [16] B. H. Cooper, B. B. L. Donniss, *Appl. Catal.*, **A** **1996**, *137*, 203–223.
- [17] H. Greenfield, *Ann. NY Acad. Sci.* **1973**, *214*, 233–242.
- [18] L. Plasseraud, G. Süß-Fink, *J. Organomet. Chem.* **1997**, *539*, 163–170.
- [19] G. Süß-Fink, M. Faure, T. R. Ward, *Angew. Chem. Int. Ed.* **2002**, *41*, 99–101.
- [20] J. D. Scholten, B. C. Leal, J. Dupont, *ACS Catal.* **2012**, *2*, 184–200.
- [21] E. T. Silveira, A. P. Umpierre, L. M. Rossi, G. Machado, J. Morais, G. V. Soares, I. J. R. Baumvol, S. R.; Teixeira, P. F. P. Fichtner, J. Dupont, *Chem. Eur. J.* **2004**, *10*, 3734–3740.
- [22] L. M. Rossi, G. Machado, *J. Mol. Catal. A: Chem.* **2009**, *298*, 69–73.
- [23] A. Gual, C. Godard, S. Castellón, C. Claver, *Dalton Trans.* **2010**, *39*, 11499–11512.
- [24] A. Nowicki, V. Le Boulaire, A. Roucoux, *Adv. Synth. Catal.* **2007**, *349*, 2326–2330.
- [25] A. Denicourt-Nowicki, A. Ponchel, E. Monflier, A. Roucoux, *Dalton Trans.* **2007**, 5714–5719.
- [26] M. Fang, N. Machalaba, R. A. Sánchez-Delgado, *Dalton Trans.* **2011**, *40*, 10621–10632.
- [27] L. Gao, K. Kojima, H. Nagashima, *Tetrahedron* **2015**, *71*, 6414–6423.
- [28] M. Kaushik, H. M. Friedman, M. Bateman, A. Moores, *RSC Adv.* **2015**, *5*, 53207–53210.
- [29] M. Takasaki, Y. Motoyama, K. Higashi, S. H. Yoon, I. Mochida, H. Nagashima, *Chem. Asian J.* **2007**, *2*, 1524–1533.
- [30] M. Zahmakıran, Y. Tonbul, S. Özkar, *J. Am. Chem. Soc.* **2010**, *132*, 6541–6549.
- [31] A. Maximov, A. Zolotukhina, L. Kulikov, Y. Kardasheva, E. Karakhanov, *Reac. Kinet. Mech. Cat.* **2016**, *117*, 729–743.
- [32] J. Huang, T. Jiang, B. Han, W. Wu, Z. Liu, Z. Xie, J. Zhang, *Catal. Lett.* **2005**, *103*, 59–62.
- [33] G. Marconi, P. Pertici, C. Evangelisti, A. M. Caporusso, G. Vitulli, G. Capannelli, M. Hoang, T. W. Turney, *J. Organomet. Chem.* **2004**, *689*, 639–646.
- [34] F. Su, L. Lv, F. Y. Lee, T. Liu, A. I. Cooper, X. S. Zhao, *J. Am. Chem. Soc.* **2007**, *129*, 14213–14223.
- [35] E. A. Karakhanov, A. L. Maksimov, A. V. Zolotukhina, S. V. Kardashev, *Petrol. Chem.* **2010**, *50*, pp. 290–297.
- [36] E. A. Karakhanov, A. L. Maksimov, A. V. Zolotukhina, M. V. Terenina, A. V. Vutolkina, *Petrol. Chem.* **2016**, *56*, 6, 491–502.
- [37] E. Karakhanov, A. Maximov, A. Zolotukhina, Y. Kardasheva, M. Talanova, *J. Inorg. Organomet. Polym.* **2016**, *26*, 1264–1279.
- [38] D. R. Rolison, *Science* **2003**, *299*, 1698–1701.
- [39] C. M. A. Parlett, K. Wilson, A. F. Lee, *Chem. Soc. Rev.* **2013**, *42*, 3876–3893.
- [40] C. Zhu, D. Du, A. Eychmüller, Y. Lin, *Chem. Rev.* **2015**, *115*, 8896–8943.
- [41] J. Zhang, C. M. Li, *Chem. Soc. Rev.* **2012**, *41*, 7016–7031.
- [42] D. Walsh, L. Arcelli, T. Ikoma, J. Tanaka, S. Mann, *Nat. Mater.* **2003**, *2*, 386–390.
- [43] G. S. Attard, C. G. Goltner, J. M. Corker, S. Henke, R. H. Templar, *Angew. Chem. Int. Ed.* **1997**, *36*, 1315–1317.
- [44] J. Erlebacher, M. J. Aziz, A. Karma, N. Dimitrov, K. Sieradzki, *Nature* **2001**, *410*, 450–453.
- [45] Y. Ding, J. Erlebacher, *J. Am. Chem. Soc.* **2003**, *125*, 7772–7773.
- [46] N. C. Bigall, A-K. Herrmann, M. Vogel, M. Rose, P. Simon, W. Carrillo-Cabrera, D. Dorfs, S. Kaskel, N. Gaponik, A. Eychmüller, *Angew. Chem. Int. Ed.* **2009**, *48*, 9731–9734.
- [47] K. G. S. Ranmohotti, X. Gao, I. U. Arachchige, *Chem. Mater.* **2013**, *25*, 3528–3534.
- [48] S. Tang, S. Vongehr, Y. Wang, J. Cui, X. Wang, X. Meng, *J. Mater. Chem. A* **2014**, *2*, 3648–3660.
- [49] K. S. Krishna, C. S. Suchand Sandeep, R. Philip, M. Eswaramoorthy, *ACS Nano* **2010**, *4*, 2681–2688.
- [50] C. Zhu, S. Guo, S. Dong, *Chem. Eur. J.* **2013**, *19*, 1104–1111.
- [51] Z. Zhu, Y. Zhai, S. Dong, *ACS Appl. Mater. Interfaces* **2014**, *6*, 16721–16726.
- [52] H. L. Jiang, Q. Xu, *Catalysis Today* **2011**, *170*, 56–63.
- [53] N. Cao, W. Luo, G. Cheng, *Int. J. Hydrogen Energy* **2013**, *38*, 11964–11972.
- [54] E. K. Abo-Hamed, T. Pennycook, Y. Vaynzof, C. Toprakcioglu, A. Koutsoubas, O. A. Scherman, *Small* **2014**, *10*, 3145–3152.
- [55] C. D. Wagner, W. M. Riggs, L. E. Davis, J. F. Moulder, G. E. Muilenberg, *Handbook of X-ray Photoelectron Spectroscopy*, Physical Electronics Division, Perkin-Elmer: Eden Prairie, MN, **1979**.
- [56] K. S. W. Sing, D. H. Everett, R. A. W. Haul, L. Moscou, R. A. Pierotti, J. Rouquerol, T. Siemieniewska, *Pure & Appl. Chem.* **1985**, *57*, 603–619.
- [57] K. Kusada, H. Kobayashi, T. Yamamoto, S. Matsumura, N. Sumi, K. Sato, K. Nagaoka, Y. Kubota, H. Kitagawa, *J. Am. Chem. Soc.* **2013**, *135*, 5493–5496.
- [58] M. H. G. Precht, M. Scariot, J. D. Scholten, G. Machado, S. R. Teixeira, J. Dupont, *Inorg. Chem.* **2008**, *47*, 8995–9001.
- [59] L. Song, X. Li, H. Wang, H. Wu, P. Wu, *Catal. Lett.* **2009**, *133*, 63–69.
- [60] C. Bianchini, V. D. Santo, A. Meli, S. Moneti, M. Moreno, W. Oberhauser, R. Psaro, L. Sordelli, F. Vizza, *J. Catal.* **2003**, *213*, 47–62.
- [61] M. Zahmakıran, Y. Tonbul, S. Özkar, *Chem. Commun.* **2010**, *46*, 4788–4790.
- [62] C. L. Young, *Solubility Data Series – Hydrogen and Deuterium*, Pergamon Press, New York, **1981** (Volume 5 and 6).
- [63] P. A. Rautanen, J. R. Aittamaa, A. O. I. Krause, *Ind. Eng. Chem. Res.* **2000**, *39*, 4032–4039.
- [64] N. Hiyoshi, C. V. Rode, O. Sato, M. Shirai, *Appl. Catal.*, **A** **2005**, *288*, 43–47.
- [65] D. J. Roddy, *Interface Focus* **2013**, *3*, 20120038.
- [66] A. Corma, S. Iborra, A. Velty, *Chem. Rev.* **2007**, *107*, 2411–2502.
- [67] J. Zakzeski, P. C. A. Bruijninx, A. L. Jongerijs, B. M. Weckhuysen, *Chem. Rev.* **2010**, *110*, 3552–3599.
- [68] C. Zhao, Y. Kou, A. A. Lemonidou, X. B. Li, J. A. Lercher, *Angew. Chem. Int. Ed.* **2009**, *48*, 3987–3990.
- [69] H. Ohta, H. Kobayashi, K. Hara, A. Fukuoka, *Chem. Commun.* **2011**, *47*, 12209–12211.
- [70] N. Yan, Y. A. Yuan, R. Dykeman, Y. A. Kou, P. J. Dyson, *Angew. Chem. Int. Ed.* **2010**, *49*, 5549–5553.
- [71] J. Y. He, C. Zhao, J. A. Lercher, *J. Am. Chem. Soc.* **2012**, *134*, 20768–20775.
- [72] X. Cui, A. E. Surkus, K. Junge, C. Topf, J. Radnik, C. Kreyenschulte, M. Beller, *Nat. Commun.* **2016**, *7*:11326, doi: 10.1038/ncomms11326.
- [73] Y. R. Luo, *Comprehensive Handbook of Chemical Bond Energies*, CRC Press, Boca Raton, FL, **2007**.
- [74] R. A. Dalla Betta, *J. Phys. Chem.* **1975**, *79*, 2519–2525.

[75] W. H. Heise, B.J. Tatarchuk, *Surf. Sci.* **1989**, 207, 297-322.

[76] P. V. Ramachandran, P. D. Gagare, *Inorg. Chem.* **2007**, 46, 7810-7817.

WILEY-VCH

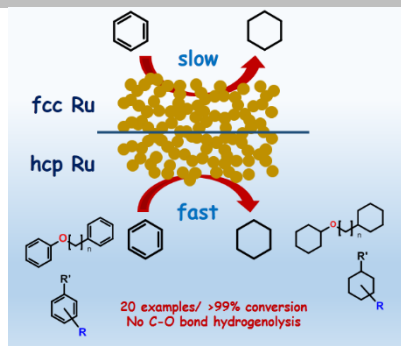
Accepted Manuscript

Layout 1:

FULL PAPER

Different phases, different

reactivity: Using one step reduction method, by a judicious choice of the reducing agents, two different phases (hcp and fcc) of ruthenium were synthesized which exhibit different catalytic activities towards benzene hydrogenation reaction under mild conditions. Further, this ruthenium catalyst was utilized for selective hydrogenation of aromatic cores of various oxygenated aromatics without C-O bond hydrogenolysis.

*Sourav Ghosh, Balaji R. Jagirdar****Page No. – Page No.****Title**